Doped and nano hybrid aluminates - A Review

H.V. Harini, H.P. Nagaswarupa*
Department of Studies in Chemistry, Shivagangothri , Davangere University, Davangere-577007
*nswarupa@davangereuniversity.ac.in

Abstract: The addition of single components to doped materials and hybrid components that have a higher impact on photocatalytic degradation applications and electrochemical research is being made possible by nanometals and metal oxides of aluminate-based nanomaterials. There are several different techniques to create aluminates. Aluminates have been characterized using X-Ray diffraction, UV-VIS, Fourier transform infrared spectroscopy (FT-IR), Scanning electron microscopy SEM, and Transmission electron microscopy (TEM). The microstructure, size, shape, and adsorption behaviour of the photocatalysts have an impact on the properties of the composite material on various surfaces. In electrochemical studies, hybrid and doped materials demonstrated good reversibility, high conductivity, high capacitance, and also showed high performance in biosensing. The most efficient and economical nanomaterial for all of the aforementioned uses is nano hybrid aluminates.

Keywords: Aluminates, Composites, Photocatalysis, Photoluminescence, Electrochemical Studies

Introduction

Aluminates are a fantastic option because of their high melting point, robust mechanical properties, and chemical stability. High specific strength, low coefficient of thermal expansion, strong corrosion resistance, and low density are some of the significant properties that permit its uses in transportation, defense, construction, energy distribution, and consumers goods. Aluminates of various types have been created, including single components, metal ion doped aluminates, nano hybrid or multi composite aluminates [1]. Spinel oxides are the most often utilised semiconductor materials in photocatalytic pollution reduction and the general chemical formula of spinel oxides is AB_2O_4, where A and B are two distinct cations with differing oxidation states. A and B are divalent and trivalent ions, respectively. Because of their unusual features, they have been used as optical materials, catalysts, and photocatalysts. The fact that band gaps and other features of this material may be easily adjusted is a huge plus [2].

Aluminates and its composites are found to be more effective for photocatalytic degradation. In single-component aluminates, photocatalytic degradation material possesses pores, low specific surface area, and active sites; the use of photocatalytic degradation of aluminates has a limited adsorption of organic dye. It has broad band gap energy and a high carrier recommendation rate [3].

From many years, spoliation of water has been a significant problem for the ecosystem. Direct flow of polluting materials into water sources from the textile, paper, pharmaceutical, and other sectors have a detrimental effect on human health. Previously screening, chemical reaction, atmospheric oxidation, physical absorption, biological methods, etc. have all been tested as ways to eliminate the pollutants from waste water but these methods failed to solve the treatment of waste water [4]. By employing various semiconductor materials, researchers have now identified that photocatalytic degradation, which will detoxify and eliminate toxins from the water can alleviate the waste water problem. Researchers are using organic dyes in water to mimick the polluted water for different types of deterioration.

Aluminates phosphors are currently the best materials that have replaced the outdated commercial afterglow phosphors containing sulphur [5, 6]. Because they have better thermal and chemical stability than sulphur-based phosphors, nano hybrid and doped aluminates are potential phosphors [7, 8]. Excitation and emission spectra have been used to investigate photoluminescence properties. These spectra can be used to determine the band gap with

the relative energy position of sub-band gap defect states in materials that can be affected by the synthesis condition [9].

In recent years, aluminates are used in a wide range of industries, including supercapacitors, sensors, electrochemical sensors, and biosensors. Aluminate-based nanoparticles are used to improve metal oxides' inferior electrical conductivity, which prevents them from being suitable materials for electrochemical sensors. The aluminates' higher electrical conductivity, high surface-to-volume ratio, and larger potential window with improved stability can be attributed to them [10, 11]. Electrochemical investigations have shown improved reversibility of the modified electrodes by aluminates in redox states. The electrode sensor shows an increased cathodic and anodic peak current.

Synthesis of Aluminates

Nano hybrid aluminates are synthesised using a variety of methods. Some review papers mention combustion, sol-gel auto combustion, hydrothermal, sonication, coprecipitation, and solgel synthesis. Many additional approaches can be used, but these are the ones that are being discussed in fig.1. Table-1 lists the various aluminates, their uses and synthesis methods.

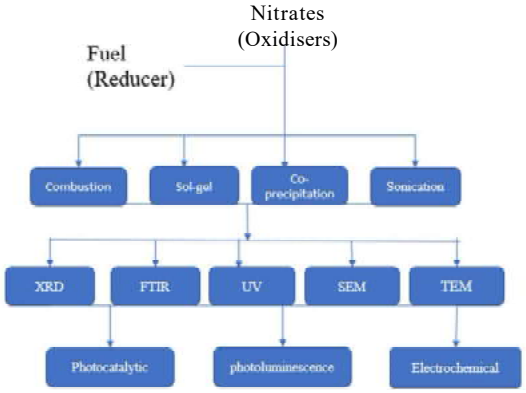


Fig 1-Synthesis, Characterisation, and Applications of Nano Aluminates

Characterisation

X-Ray diffraction is used to determine the crystallinity of the samples and phase purity. UV-VIS-spectroscopy is used to study the absorbance of the sample. - Scanning electron microscopy (SEM) shows the morphology of the samples and also about agglomeration of sample, Transmission electron microscopy (TEM) it is used to find the size of the sample while FTIR stands for Fourier transform infrared spectroscopy, which reveals the information about functional groups present in the material. These are the terms used in the papers that have been recommended.

Aluminate-based nanomaterials typically undergo XRD analysis to examine their crystal structure and elemental composition. $BaMgAl_{10}O_{17}$ (BMA) nanomaterial which is synthesized by combustion method by using aloe vera extract with an aluminate basis, as showed in its XRD spectrum[12].

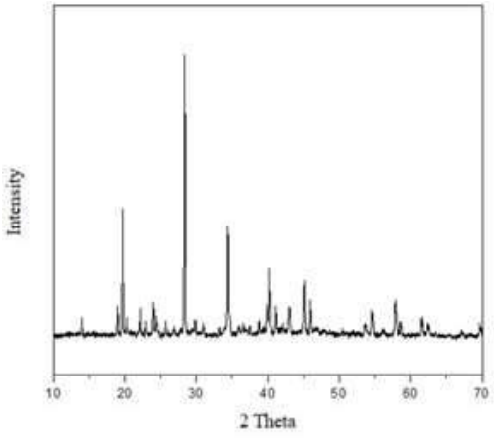


Fig.2 XRD patterns of BMA NPs of Aluminates

Aluminate-based nanomaterials typically undergo XRD analysis to investigate their crystal structure and elemental composition. As shown in figure 2, the XRD spectrum of the nano hybrid aluminates material showed peaks at (111), (103), (104), (110), (114), (220), (412), (511), (440), and (209), and the pattern recorded by the XRD method is in good agreement with the standard pattern for hexagonal correlated with the data of $BaMgAl_{10}O_{17}$-(JCPDS 26-0136) figure 2, (12).

Table 1: Different types of Synthesized, Doped and Nano Hybrid Aluminates

Sl.no	Nano hybrid Aluminate NPs	Morphology size	Applications	Synthesis Method	Reference
1	$BaMgAl_{10}O_{17}$ nanoparticle	7 nm	Photocatalytic activities, antimicrobial activity, cyclic voltammetry analysis	solution combustion	12
2	Aluminium oxide nano particles (Al_2O_3 NPs)	6 -16 nm	photocatalytic, and electrochemical sensor	sonication method	13
3	$NdAlO_3$-Al_2O_3	10-12 nm	Structural and Optical Properties	sol-gel process	14
4	Magnesium aluminate spinel ($MgAl_2O_4$)	40 nm	Characteristics	Coprecipitation method, sol–gel process	15
5	$MgAl_2O_4/CeO_2/Mn_3O_4$ nanoparticles		Photocatalytic activity	Sonication method	16
6	$Ca_3MgAl_{10}O_{17}$ nano-particle	20 to 25 nm	Photocatalytic and non-enzymatic sensor	chemical combustion method	17
7	$CaMgAl_{10}O_{17}$**:Ce^{3+}**	42 nm	Optical properties	Combustion method	18
8	$Cu_2ZnAl_2O_4$nanoparticle	40 nm	photocatalytic, and electrochemical sensor	Combustion method	19

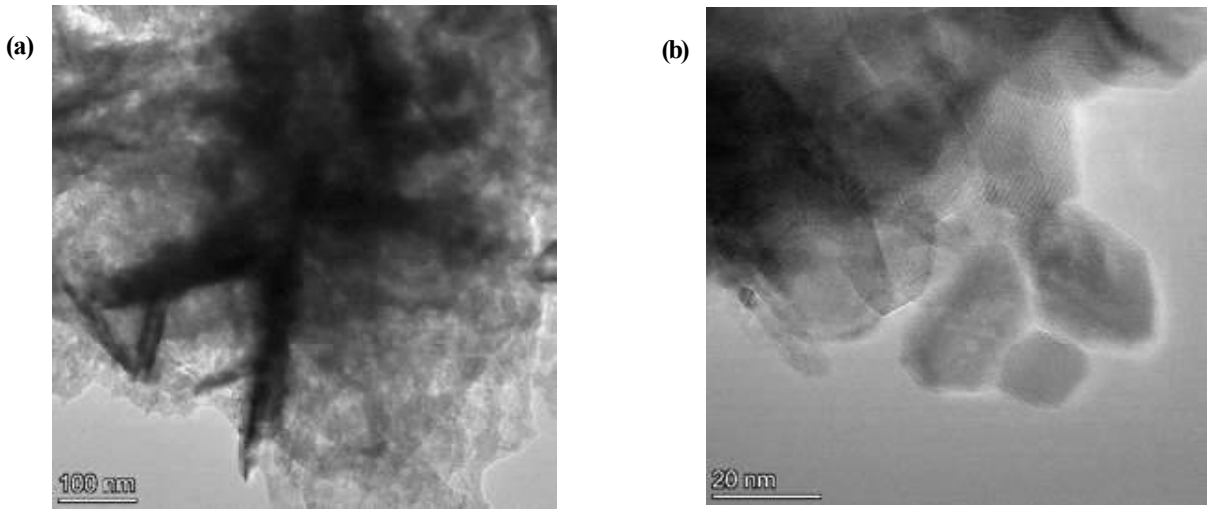


Fig 3. (a, b) The TEM images of BMA NPs

The solution combustion approach was used to create BMA NPs, and TEM micrographs of these particles demonstrate that their micrographic structure is not disseminated evenly, with bigger agglomerations occurring in small-sized particles (figure 3-(a,b)). Additionally, it was discovered to have excellent crystallinity [12].

Application

Photocatalytic Activity

In order to create a new photocatalyst with increased charge transfer capacity and separation efficiency, metals are combined with suitable single-component aluminates to create new nano hybrid aluminates. This increases the specific surface area of the new photocatalyst, which improves the accessibility of the pollutant molecules to the active sites and boosts photocatalytic activity than the single component.

Composite photocatalyst leverages the advantages of each component catalyst to generate a new composite photocatalyst with improved photocatalytic activity. Among the ways for raising electron-hole pair separation and reducing recombination rate, developing the composite structure is a useful strategy for boosting photocatalytic activity. When an n-type semiconductor is linked with a p-type semiconductor, the recombination of photo-induced electron-hole pairs is limited because an electric field is created. When an n-type and a p-type semiconductor are coupled together, electron and hole diffusion in the interface of the two semiconductors creates an electric field, allowing for higher separations of photo-excited electron hole pairs [20-22]. $MgAl_2O_4$-AC has demonstrated an interaction between materials that enhances charge carrier separation, which improves physicochemical properties and improves photocatalytic performance. $SrAl_2O_4$: Eu, Dy/SiO_2 composite photocatalysts like n-n or p-n junction composites are selectivity through synergistic catalytic effects between different materials. Heterojunctions are a useful method for identifying compounds with great selectivity and sensitivity, which have a number of benefits. Continuous p-n heterojunction photocatalysts, which can only respond to ultraviolet (UV) light and have low charge mobility and separation efficiency, could significantly improve photocatalytic activity and multicomponent composite photocatalysts [23-30].

In Table 2, $BaMgAl_{10}O_{17}$ of photocatalytic degradation that demonstrated an increase in effectiveness with UV light irradiation period and Acid Red 88 dye. According to the AR88 dye's performance, 97% of the dye degraded after 120 minutes, and 95% of the dye degraded effectively within the half-life and 50% within 22.80 minutes, which showed excellent efficiency of degradation [12]. $Cu_2ZnAl_2O_4$ is created through the combustion process, which has been carried out in the presence of three distinct sources, including UV light, sunlight, and darkness, with results of 91.3%, 63.22%, and 3.1%, respectively. The amount of dye molecules that bind to the surface of the photocatalyst is reduced when dye concentration rises, and dye concentration also exhibits greater photo-decolorization activities [19]. $Mg_xNi_{1-x}Al_2O_4$here this confirmed that compared to metal oxides, the doped oxides will show higher efficiency. It had showed 99.3% of degradation with Congo red at 90 mins irradiated with UV light [2]. Compared to pure g-C_3N_4 the supported $SrA_{l2}O_4$:Eu,Dy showed a good performance of degradation. The low amount of SiO_2 binding reagent has improved the degradation which has higher efficiency with methylene blue 90% at 60 mins [31].

Mechanism of degradation

Figure 4 explains the electrons in the valence band (VB) are energised and migrate to the conduction band (CB), generating an equal number of holes (positive charges) in the VB. The electrons produced in the conduction band are carried to the catalyst, where they combine with ambient O_2 to produce superoxide radicals (O^-_2). Simultaneously, the holes in the VB will react with water (H_2O) to form hydroxyl radicals (OH^-). These radicals will react with the dye and eventually break the dye molecules, causing the dye to degrade.

Table 2: Photocatalytic degradation of Doped and Nano Hybrid Aluminates

SAMPLE	DYES	LAMP	TIME(min) `	% DECOMPOSED	REFERENCE
$Mg_{0.9}Ni_{0.1}Al_2O_4$	Congo red	UV light	90	99.3	2
$Bi_7O_9I_3$-$MgAl_2O_4$	Methylene blue	Sun light	120	95.9	4
$BaMgAl_{10}O_{17}$	Acid Red 88	UV irradiation	120	95	12
$Ca_3MgAl_{10}O_{17}$	Acid orange-88	UV irradiation	120	92.25	17
$Cu_2ZnAl_2O_4$	Acid Red 88	UV light, sunlight, and dark	120	91.3, 63.22, and 3.1	19
$MgAl_2O_4$-AC	Methylene blue	Solar light	140	96	30
g-C_3N_4/$SrAl_2O_4$: Eu,Dy/SiO_2	Methylene blue	300 W Xe lamp	60	90	31
g-C_3N_4@Au@ $SrAl_2O_4$: Eu,Dy/Composite	Rhodamine B	300 W Xe lamp	120	80	32
g-C_3N_4@NiAl-LDH (layered double hydroxide)	Methy orange	Visible light	180	99	33
TiO_2/MgZnAl LDH (layered double hydroxide)	Rhodamine B	Visible Light	9 hrs	93.73	34

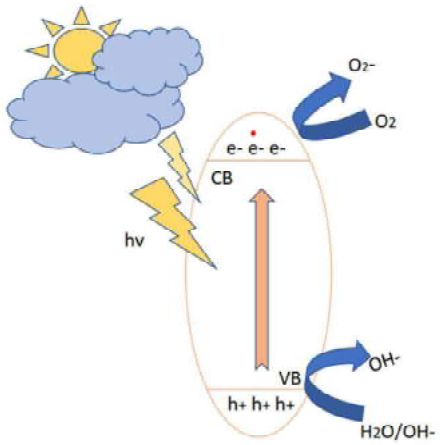


Fig 4: Schematic representation of photocatalytic degradation

Photoluminescence studies

Photoluminescence (PL) studies were used to look at the types of trapping centres found in the crystal lattice. The photoluminescence of doped aluminate found that the presence of rarer elements produces unique light emissions. Where the emission is strong or weak bands will be indicated by the light emission.

$CaMgAl_{10}O_{17}$ with phosphor Ce^{3+} exhibits two distinct colour areas; the peak positions remain unchanged, when the dopant concentration rises, but the peak intensities decline. These limits of the compound exhibit multipolar and dipole dipole interaction. For every $MMgAl_{10}O_{17}$,(M= Ca) the Ce^{3+} ion separates into levels 2f7/2 and 2f5/2 of the 4f ground state. As a result, spin orbit coupling produces the blue region and red region, respectively, due to crystal field and covalency effect [18].

To show the emission band prominent due to Ce^{3+}, $CaAl_2O_4$ was co-doped with Tb^{3+} and Ce^{3+} (0.1 mol percent) phosphor. The PL emission spectra of the Ce^{3+} doped and Ce^{3+} | Tb^{3+} co-doped samples do not show a noticeable change. The only variation that can be distinguished in the Ce-Tb co-doped sample is the appearance of a small peak in the emission spectrum at 467 nm. Possible causes include Tb^{3+} emission (5D4 -7F6). This suggests that there is no overlap between Tb^{3+} excitation and Ce^{3+} emission. It is evident that the co-doped sample's emission centres are solely composed of Ce^{3+} ions [35].

$CaAl_2O_4$:Eu^{2+}, Dy^{3+} phosphor is more abundant than the other created phosphors due to its single monoclinic phase, which possesses ideal tetrahedral compact $CaAlO_4$ structures and allows for the efficient reduction of Eu^{3+} to Eu^{2+}, which results in a high photoluminescence intensity. $CaAl_2O_4$:Eu^{2+}, Dy^{3+} phosphor therefore has the highest photoluminescence intensity. Because there are two alternative metal aluminate lattices available, $CaBaAl_2O_4$:Eu^{2+}, Dy^{3+}, and $CaMgAl_2O_4$:Eu^{2+}, Dy^{3+} phosphors displayed lower intensity because completely tetrahedral structures were not formed [36].

Electrochemical studies

Using a potentiostate with a traditional three electrode system, synthetic aluminates' conduction capacity and charge transfer resistance were tested fig.3. The electrolyte used was solution, and the working electrode was a carbon paste electrode that had been prepared. The reference electrode was Ag/AgCl, and the counter electrode was platinum. Voltage was applied to determine the material's oxidation and reduction peaks. At various points in the rate system, the cyclic voltammetry plot clearly depicts a reduction peak and an oxidation peak. The charge efficiency and reversibility of the electrode reaction at room temperature can also be determined using CV [37]. The produced electrode material was subjected to electrochemical impedance spectroscopy (EIS), which assesses the separation efficiency between the charge carriers generated based on the charge transfer resistance and the electrical conductivity. This illustrates how the produced electrode material penetrated the electrolyte medium and clarified the areal capacitance [38,39]. In Explained by the Nyquist plot is the nature of the electrode in impedance. The value of the high-frequency region curve linearly varies with the diameter of the semi-circular arc and represents the charge transfer processes taking place at the electrode-electrolyte interfaces. On the other hand, the electrode capacitance is measured by the low-frequency region linear curve [40-42].

Electrochemical sensors based on aluminate nanomaterials have been used to detect and quantify a variety of chemical species, including hydrogen oxide in human blood, paracetamol, glucose, and water contaminants like arsenic, lead, mercury, tin. Electrical signals produced from CVs and EIS techniques were typically used to analyse the detection performance of aluminate-supported nanomaterial electrochemical sensors for the species. As a way to quantitatively detect the analyte.

Paracetamol is one of the most often used medications in the world, Because of its effectiveness against fever, colds, and flu as well as its high activity against mild to moderate pain associated with arthritis, backaches, and headaches. Generally speaking, it doesn't have any negative side effects, but in rare instances, hypersensitivity or overdosing can result in the creation of toxic metabolites that can cause severe nephrotoxicity and hepatotoxicity. Standard doses may also result in liver failure. [43-46]. Barium magnesium aluminate (BMA) is with smaller nanostructures increased the electrode's resistance to charge transfer. In order to efficiently lower the material's internal resistance, the electrolyte ions intercalate and de-intercalate within the accessible surface area [12].

A sugar generated from starch that is equivalent to glucose, dextrose is crucial for the blood's supply of carbohydrates. It provides the energy needed for human activity. Establishing and maintaining control of blood is essential because it plays a part in the onset and development of diabetes mellitus, which causes death worldwide. Enzyme sensors and non-enzymatic sensors are the two different kinds of glucose sensors used. Changes in temperature and pH levels render enzyme sensors inactive. As a result, non-enzymatic glucose sensors are now often utilised to detect and measure glucose [47,48]. When sensing dextrose, the oxidation and reduction peaks, They have a greater surface area and number of electrochemical active sites, increased charge conductivity and speedy charge transfer, and electrodes with good reversibility and high conductivity and high capacitance. The results of the electrochemical tests showed that this electrode has the potential to be a very useful electrode material for detecting dextrose and a few specific metals in an alkaline media. These attributes enable them to function as an efficient electrochemical glucose sensor [17].

Lead and tin continue to be one of the most hazardous poisonous heavy metals. The guidelines for potential health impacts are directly connected to measured blood Pb levels, and despite great efforts to detect and reduce heavy metal exposure sources, this metal still poses a serious health risk. There is a great deal of interest in finding alternative lead and tin biomarker matrices, such as plasma/serum, saliva, bone, teeth, faeces, and urine, which may offer a stronger association with unfavourable health effects [49].

$Cu_2ZnAl_2O_4$ has surface qualities that are more homogeneous, have a high degree of crystalline availability, and had a large amount of surface area, which offers more active sites. With increased scan rate, the anodic and cathodic peak positions altered, and electron transfer kinetics also became better. The cyclic voltammogram of the lead sensors, however, that the oxidation peak has additional peaks whereas the reduction peak does not. Likewise, there are three additional peaks on the anodic side and one additional peak on the cathodic side for tin [19].

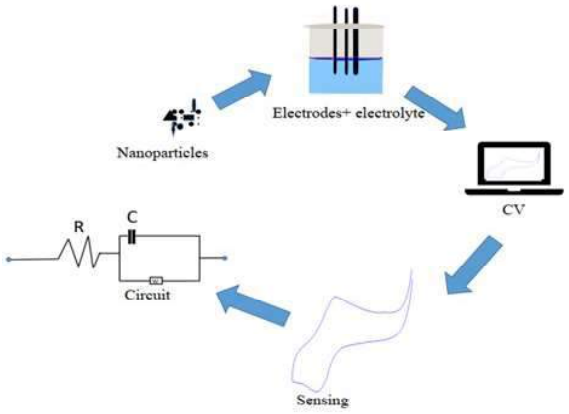


Fig 5: Schematic representation of electrochemical studies

Conclusion

Aluminate-based photocatalysts are a type of photocatalyst that has grown in popularity in recent years. The use of numerous heterojunction composites to combine the benefits of several semiconductor materials and improve photocatalytic activity is advantageous. The band gap of single component aluminates is relatively broad, making it

difficult to respond to visible light. As a result, for the creation of multi component photocatalysts, semiconductor materials that can respond to visible light are preferred. A photocatalyst was created by mixing several semiconductor materials, and its photocatalytic activity was proven by multi composite aluminates with outstanding performance and a higher tendency of waste water degradation. Modern electrochemical sensors built on aluminate materials were created, and they are continually being improved and functionalized, to find and identify different analyte species. better stability on the electrochemical oxidation of the sample specie, improved electrical conductivity, higher electrocatalytic sensitivity and selectivity.

Reference

1. Lampman, S. R., & Zorc, T. B. (1990). ASM Handbook Volume 02: Properties and Selection: Nonferrous Alloys and Special-Purpose Materials. *Materials Park, Ohio, USA: ASM International*, 1592-1633.

2. Hajavazzadeh, R., Kargar Razi, M., & Mahjoub, A. R. (2021). Synthesis and characterization of Mg1-xNixA_{l2O4} and their photocatalytic behaviors towards Congo red under UV light irradiation. *International Journal of Nano Dimension*, *12*(1), 67-75.

3. Li, J., Wang, S., Sun, G., Gao, H., Yu, X., Tang, S., ... & Wei, Y. (2021). Facile preparation of $MgA_{l2O4}/Ce_{O2}/Mn_3O_4$ heterojunction photocatalyst and enhanced photocatalytic activity. *Materials Today Chemistry*, *19*, 100390.

4. Abbasi Asl, E., Haghighi, M., & Talati, A. (2019). Sono-solvothermal fabrication of flowerlike $Bi_7O_9I_3$-MgA_{l2O4} p-n nano-heterostructure photocatalyst with enhanced solar-light-driven degradation of methylene blue. *Solar Energy*, *184*(Complete), 426–439. https://doi.org/10.1016/j.solener.2019.04.012

5. Cheng, B., Zhang, Z., Han, Z., Xiao, Y., & Lei, S. (2011). SrAlxO y: Eu 2+, Dy 3+(x= 4) nanostructures: Structure and morphology transformations and long-lasting phosphorescence properties. *CrystEngComm*, *13*(10), 3545-3550.

6. Si, D., Geng, B., & Wang, S. (2010). One-step synthesis and morphology evolution of luminescent Eu^{2+} doped strontium aluminate nanostructures. *CrystEngComm*, *12*(10), 2722-2727.

7. Wiglusz, R. J., Grzyb, T., Lukowiak, A., G³uchowski, P., Lis, S., & Strek, W. (2012). Comparative studies on structural and luminescent properties of Eu3+: $MgAl_2O_4$ and Eu3+/Na+: $MgAl_2O_4$ nanopowders and nanoceramics. *Optical Materials*, *35*(2), 130-135.

8. Wiglusz, R. J., & Grzyb, T. (2011). The effect of Tb^{3+} doping on the structure and spectroscopic properties of $MgAl_2O_4$ nanopowders. *Optical Materials*, *33*(10), 1506-1513.

9. Anand, G., L, J. & Vijaya, J. (2013). Microwave combustion synthesis, structural, optical and magnetic properties of Zn^{1-x}CoxAl2O4 ($0 \leq x \leq 0.5$) spinel nanostructures. *Journal of Alloys and Compounds*, 581:558–566

10. X.-F. Zhang et al, Solvothermal synthesis of N-doped graphene supported Pt Conanodendrites with highly catalytic activity for 4-nitrophenol reduction, Appl.Surf. Sci. 428 (2018) 798–808.

11. X. Wu et al, Graphene-supported ordered mesoporous composites used for environmental remediation: A review, Sep. Purif. Technol. 239 (2020) 116511.

12. Vasudha, M., Gayathri, D., Gurum, S. S., Kavya, M. R., Nagaswarupa, H. P., Surendra, B. S., ... & Prathapkumar, C. (2021). Synthesis of BMA NPs using aloe vera gel for their electrochemical, biological and photocatalytic studies. *Journal of Photochemistry and Photobiology*, *6*, 100017.

13. Kusuma, K. B., Manju, M., Ravikumar, C. R., Nagaswarupa, H. P., Amulya, M. S., Anilkumar, M. R., ... & Ravikantha, N. (2020). Photocatalytic and electrochemical sensor for direct detection of paracetamol comprising ã-aluminium oxide nanoparticles synthesized via

sonochemical route. *Sensors International*, *1*, 100039.

14. Mathur, S., Veith, M., Shen, H., Hüfner, S., & Jilavi, M. H. (2002). Structural and optical properties of NdAlO3 nanocrystals embedded in an Al_2O_3 matrix. *Chemistry of materials*, *14*(2), 568-582.

15. Guo, J., Lou, H., Zhao, H., Wang, X., & Zheng, X. (2004). Novel synthesis of high surface area $MgAl_2O_4$ spinel as catalyst support. *Materials Letters*, *58*(12-13), 1920-1923.

16. Li, J., Wang, S., Sun, G., Gao, H., Yu, X., Tang, S., ... & Wei, Y. (2021). Facile preparation of $MgAl_2O_4/CeO_2/Mn_3O_4$ heterojunction photocatalyst and enhanced photocatalytic activity. *Materials Today Chemistry*, *19*, 100390.

17. Vasudha, M., Khan, A. A., Bhumika, K. M., Gayathri, D., Nagaswarupa, H. P., Raghavendra, N., ... & Surendra, B. S. (2021). Facile chemical synthesis of $Ca_3MgAl10O17$ nanomaterials for photocatalytic and non-enzymatic sensor applications. *Sensors International*, *2*, 100082.

18. Selot, A., Aynyas, M., Tiwari, M., & Dev, K. (2014, April). Synthesis, characterization and optical properties of Ce^{3+} activated $CaMgAl_{10}O_{17}$ phosphor. In *AIP Conference Proceedings* (Vol. 1591, No. 1).

19. Harini, H. V., Nagaswarupa, H. P., Bekele, E. T., Murthy, H. A., & Ravikumar, C. R. (2022). Novel synthesis of $Cu2ZnAl_2O_4$ nanostructures for photocatalytic and electrochemical sensor applications. *Sensors International*, 100225.

20. Fan, J. M., Zhao, Z. H., Gong, C., Xue, Y. Q., & Yin, S. (2018). Persistent methyl orange degradation ability of $MgAl_2O_4$:(Pr3+, Dy3+)/ M-TiO2 luminescent photocatalyst. *Journal of Nanoscience and Nanotechnology*, *18*(3), 1675-1681.

21. Asl, E. A., Haghighi, M., & Talati, A. (2020). Enhanced simulated sunlight-driven magnetic $MgAl_2O_4$-AC nanophotocatalyst for efficient degradation of organic dyes. *Separation and Purification Technology*, *251*, 117003.

22. Woo, H. S., Na, C. W., Kim, I. D., & Lee, J. H. (2012). Highly sensitive and selective trimethylamine sensor using one-dimensional ZnO–Cr2O3 hetero-nanostructures. *Nanotechnology*, *23*(24), 245501.

23. Staerz, A., Kim, T. H., Lee, J. H., Weimar, U., & Barsan, N. (2017). Nanolevel control of gas sensing characteristics via p–n heterojunction between Rh_2O_3 clusters and WO3 crystallites. *The Journal of Physical Chemistry C*, *121*(44), 24701-24706.

24. Kim, T. H., Kwak, C. H., & Lee, J. H. (2017). NiO/NiWO4 composite yolk–shell spheres with nanoscale NiO outer layer for ultrasensitive and selective detection of subppm-level p-Xylene. *ACS applied materials & interfaces*, *9*(37), 32034-32043.

25. Kim, B. Y., Ahn, J. H., Yoon, J. W., Lee, C. S., Kang, Y. C., Abdel-Hady, F., ... & Lee, J. H. (2016). Highly selective xylene sensor based on NiO/NiMoO4 nanocomposite hierarchical spheres for indoor air monitoring. *ACS applied materials & interfaces*, *8*(50), 34603-34611.

26. Yoon, J. W., Kim, J. S., Kim, T. H., Hong, Y. J., Kang, Y. C., & Lee, J. H. (2016). A new strategy for humidity independent oxide chemiresistors: dynamic self refreshing of In2O3 sensing surface assisted by layer by layer coated CeO2 nanoclusters. *Small*, *12*(31), 4229-4240.

27. Wu, K., Wang, X. Y., Guo, L. L., Xu, Y. J., Zhou, L., Lyu, Z. Y., ... & Yan, C. H. (2020). Facile synthesis of Au embedded CuO_x-CeO2 core/shell nanospheres as highly reactive and sinter-resistant catalysts for catalytic hydrogenation of p-nitrophenol. *Nano Research*, *13*(8), 2044-2055.

28. Kim, J. H., Jeong, H. M., Na, C. W., Yoon, J. W., Abdel-Hady, F., Wazzan, A. A., & Lee, J. H. (2016). Highly selective and sensitive xylene sensors using Cr2O3-ZnCr2O4 hetero-nanostructures prepared by galvanic

replacement. *Sensors and Actuators B: Chemical*, *235*, 498-506.

29. Kwak, C. H., Woo, H. S., & Lee, J. H. (2014). Selective trimethylamine sensors using Cr_2O_3-decorated SnO_2 nanowires. *Sensors and Actuators B: Chemical*, *204*, 231-238.

30. Asl, E. A., Haghighi, M., & Talati, A. (2020). Enhanced simulated sunlight-driven magnetic MgAl2O4-AC nanophotocatalyst for efficient degradation of organic dyes. *Separation and Purification Technology*, *251*, 117003.

31. Mavengere, S., & Kim, J. S. (2020). Photocatalytic Properties of g-C3N4–Supported on the $SrAl_2O_4$: Eu, Dy/SiO2. *Coatings*, *10*(10), 917.

32. Liu, X., Chen, X., Li, Y., Wu, B., Luo, X., Ouyang, S., ... & Lin, J. (2019). AgC 3 N 4@ Au@ $SrAl_2O_4$: Eu 2+, Dy 3+ composite as an efficient plasmonic photocatalyst for round-the-clock environmental purification and hydrogen evolution. *Journal of Materials Chemistry A*, *7*(32), 19173-19186.

33. Salehi, G., Abazari, R., & Mahjoub, A. R. (2018). Visible-light-induced graphitic–C3N4@ nickel–aluminum layered double hydroxide nanocomposites with enhanced photocatalytic activity for removal of dyes in water. *Inorganic Chemistry*, *57*(14), 8681-8691.

34. Zhao, G., Zou, J., Li, C., Yu, J., Jiang, X., Zheng, Y., ... & Jiao, F. (2018). Enhanced photocatalytic degradation of rhodamine B, methylene blue and 4-nitrophenol under visible light irradiation using TiO2/MgZnAl layered double hydroxide. *Journal of Materials Science: Materials in Electronics*, *29*(8), 7002-7014.

35. Madhukumar, K., Rajendra Babu, K., Ajith Prasad, K. C., James, J., Elias, T. S., Padmanabhan, V., & Nair, C. M. K. (2007). Luminescence studies of rare earth doped calcium aluminate phosphors. *International Journal of Modern Physics B*, *21*(12), 1971-1980.

36. Singh, D., Kadyan, S., Ishwar Singh, P., Tanwar, V., P Simantilke, A., & Mari, B. (2016). Rapid synthesis and photoluminescent characterization of MAl_2O_4: Eu2+, Dy3+ (M= Ca/Ca+ Ba/Ca+ Mg) blue nanophosphors for white lighting display applications. *Advanced Materials Letters*, *7*(1), 47-53.

37. Shetty, K., Nagaswarupa, H. P., Rangappa, D., Anantharaju, K. S., Surendra, B. S., & Kumar, A. (2018). Comparison study of solgel and combustion method for synthesis nano spinel $MgFe_2O_4$ and its influence on electrochemical activity. *Materials Today: Proceedings*, *5*(10), 22362-22367.

38. Surendra, B. S., Nagaswarupa, H. P., Hemashree, M. U., & Khanum, J. (2020). Jatropha extract mediated synthesis of $ZnFe_2O_4$ nanopowder: Excellent performance as an electrochemical sensor, UV photocatalyst and an antibacterial activity. *Chemical Physics Letters*, *739*, 136980.

39. Kumar, C. R., Santosh, M. S., Nagaswarupa, H. P., Prashantha, S. C., Yallappa, S., & Kumar, M. A. (2017). Synthesis and characterization of â-Ni $(OH)_2$ embedded with MgO and ZnO nanoparticles as nanohybrids for energy storage devices. *Materials Research Express*, *4*(6), 065503.

40. Ranjitha, R., Bhatt, A.S., Ravikumar, C.R., Santosh, M.S., Jayanna, B.K., Nagaswarupa, H.P., Sakai, K., & Madhyastha, H. (2019). Electroactive Li incorporated cobalt oxide nanostructures for photocatalytic applications. *Materials Research Express, 6*.

41. Kumar, M. A., Ravikumar, C. R., Nagaswarupa, H. P., Purshotam, B., Gonfa, B., Murthy, H. A., ... & Tadesse, S. (2019). Evaluation of bi-functional applications of ZnO nanoparticles prepared by green and chemical methods. *Journal of Environmental Chemical Engineering*, *7*(6), 103468.

42. Avinash, B., Ravikumar, C. R., Kumar, M. A., Nagaswarupa, H. P., Santosh, M. S., Bhatt, A. S., & Kuznetsov, D. (2019). Nano CuO: Electrochemical sensor for the determination of paracetamol and D-glucose. *Journal of Physics and Chemistry of Solids*, *134*, 193-200.

43. Fatibello-Filho, O., Lupetti, K. O., & Vieira, I. C. (2001). Chronoamperometric determination of paracetamol using an avocado tissue (Persea americana) biosensor. *Talanta*, *55*(4), 685-692.

44. Afkhami, A., Khoshsafar, H., Bagheri, H., & Madrakian, T. (2014). Preparation of NiFe2O4/graphene nanocomposite and its application as a modifier for the fabrication of an electrochemical sensor for the simultaneous determination of tramadol and acetaminophen. *Analytica chimica acta*, *831*, 50-59.

45. Beitollahi, H., Raoof, J. B., & Hosseinzadeh, R. (2011). Fabrication of a nanostructure-based electrochemical sensor for simultaneous determination of N-acetylcysteine and acetaminophen. *Talanta*, *85*(4), 2128-2134.

46. Martin, F. L., & McLean, A. E. (1998). Comparison of paracetamol-induced hepatotoxicity in the rat in vivo with progression of cell injury in vitro in rat liver slices. *Drug and chemical toxicology*, *21*(4), 477-494.

47. Jeong, H., Kwac, L. K., Hong, C. G., & Kim, H. G. (2021). Direct growth of flower like-structured CuFe oxide on graphene supported nickel foam as an effective sensor for glucose determination. *Materials Science and Engineering: C*, *118*, 111510.

48. Luo, S., Chen, Y., Xie, A., Kong, Y., Wang, B., & Yao, C. (2014). Nitrogen doped graphene supported Ag nanoparticles as electrocatalysts for oxidation of glucose. *ECS Electrochemistry Letters*, *3*(11), B20.

49. Yantasee, W., Lin, Y., Hongsirikarn, K., Fryxell, G. E., Addleman, R., & Timchalk, C. (2007). Electrochemical sensors for the detection of lead and other toxic heavy metals: the next generation of personal exposure biomonitors. *Environmental health perspectives*, *115*(12), 1683-1690.